

SILK FIBROIN-BASED ANASTROZOLE NANOPARTICLE LOADED *IN SITU* INJECTABLE: DEVELOPMENT AND CHARACTERIZATION

ARFA NASRINE* , MOHAMMED GULZAR AHMED , SOUMYA NARAYANA 

Department of Pharmaceutics, Yenepoya Pharmacy College and Research Centre, Yenepoya (Deemed to be University), Mangaluru-575018, India

*Email: arfanasrine14@gmail.com

Received: 20 Feb 2023, Revised and Accepted: 28 Mar 2023

ABSTRACT

Objective: The study aims to find a suitable method of developing silk fibroin-based anastrozole nanoparticles and formulate *in situ* injectables by loading the optimized nanoparticle formulation for the sustained release treatment of breast cancer.

Methods: The nanoparticles were formulated utilizing two different methods, solvent change and precipitation approach using silk fibroin. Prepared nanoparticles characterized in terms of size, zeta potential, polydispersity, and entrapment efficiency. The chosen optimized formulation (SF-ANS-NPs-1) was subsequently analyzed for compatibility investigations by Fourier-transform infrared spectroscopy (FT-IR), thermal analysis, surface morphology, x-ray diffraction, transmission electron spectroscopy, cumulative drug release, and stability studies as per ICH guidelines. Followed by formulating and evaluating *in situ* injectable gel using pluronic F-127.

Results: A particle size of 181.70 ± 1.3 nm was reported by the optimized SF-ANS-NPs-1 formulation. FT-IR and thermal studies confirmed the compatibility of the drug with the polymers, and x-ray diffraction studies indicated crystalline nature. Surface morphology analysis indicated nano-size particle formation. A cumulative drug release (%CDR) of 94.15% was noted at the 168th hour. The results of the stability studies were indicated to be consistent over 90 d. *In situ* gel formulation showed desired spreadability, sol-gel transition temperature (37 ± 0.5 °C), viscosity (9.37 ± 1.2 mPa·s), desired acidic pH, and a sustained release for 21 d (98.11%) with three months accelerated stability.

Conclusion: The results suggested that the combination of anastrozole with silk fibroin in the form of nanoparticles and *in situ* gelling systems could be an undoubtedly effective delivery method for prolonging breast cancer therapy.

Keywords: Breast cancer, Anastrozole, Silk fibroin, Nanoparticulate drug delivery system, Thermo-responsive gelling system, *In situ* gelling injectable, Thermo-responsive gel, Sustained release drug delivery

© 2023 The Authors. Published by Innovare Academic Sciences Pvt Ltd. This is an open access article under the CC BY license (<https://creativecommons.org/licenses/by/4.0/>)
DOI: <https://dx.doi.org/10.22159/ijap.2023v15i3.47593>. Journal homepage: <https://innovareacademics.in/journals/index.php/ijap>

INTRODUCTION

Breast cancer in women is a significant global health consequence. In both industrialised and developing nations, it is the most prevalent kind of cancer in women. In 2018, breast cancer accounted for 25.4% of all cancer cases worldwide [1]. Recent research has revealed that estrogens significantly contribute to the growth of both normal and neoplastic breast epithelium. Epidemiological studies have just lately verified their long-held theories about their potential significance as breast carcinogens. Almost 74% of breast cancers (BC) are classified as estrogen receptor (ER) positive, according to cancer research. More than twenty oral antineoplastics have received approval in the US, and many more are in development. Tamoxifen adjuvant therapy was one of the first long-term oncologic treatments for hormone receptor-positive breast cancer. It lowers long-term breast cancer mortality by one-third to one-half when taken for a prolonged period [2–4]. The more recent aromatase inhibitors anastrozole (ANS), letrozole, and exemestane cut cancer recurrence by an extra 50% but must be taken for at least five to ten years [5]. Sadly, many breast cancer patients prescribed long-term oral medicines find it challenging to comply with them [6, 7].

A novel formulation that can deliver a prolonged medication release to the targeted location can be designed to circumvent these obstacles.

Numerous research has been dedicated to developing sustained and regulated drug delivery systems over the past 30 y. Over the past few years, *in situ* polymeric delivery system development has drawn much interest. By taking into account the research findings, nanoparticle (NP) based *in situ* gelling was considered for the formulation. In recent decades, nanocarriers have been crucial in a number of cancer therapies as compared to free pharmaceuticals [8]. This system has several benefits, including ease of administration, decreased frequency of administration, improved patient comfort and compliance, delivery of an accurate dose, and the ability to extend the

residence time of the drug in contact with the mucosa. These issues are typically associated with semisolid dosage forms [9, 10].

A naturally occurring protein from the Bombyx mori silkworm is called as silk fibroin (SF). The glands of arthropods like silkworms, spiders, scorpions, mites, and bees typically contain protein polymers called silks. Afterward, these arthropods spin these protein polymers into threads as they go through their metamorphosis [11, 12]. SF was first used as a biomaterial hundreds of years ago when it was used as sutures to cure wounds. SF-based biomaterials have been discovered to be helpful for a range of applications, including medication administration, because of their outstanding performance [13]. Hence the present study was planned to find out an appropriate method to formulate biodegradable SF-based ANS NPs and incorporate them to prepare *in situ* injectables as a prolong-release drug delivery system for the treatment of breast cancer.

MATERIALS AND METHODS

Materials

Anastrozole was received from Cipla Ltd. in Bangalore as a gift sample. A sample of silk fibroin was received as a gift from Sericare, a unit of Bangalore's Healthline Pvt. Ltd. D-mannitol and ethanol were purchased from Chang-shu Hongsheng and Loba Chemie Pvt Ltd in Mumbai, India (Fine Chemical Co. Ltd). Pluronic®F-127 was obtained from Sigma-Aldrich (Bangalore) and used as received. For the entire study, analytical-grade chemicals were used without further purification.

Methods

Solvent precipitation method

The mixture included an appropriate 6:4 (v/v) ratio of SF solution to ethanol. For instance, 6 ml of 0.05% (w/v) SF solution was mixed with 4 ml of ethanol or 4 ml of 0.1 mg/ml SF-ethanol in 15-mL falcon

tubes. To serve as a stabilizing agent, D-mannitol was added. The mixture was briefly vortexed, flash-frozen in liquid nitrogen, and then left to thaw at room temperature. After thawing, the obtained samples were centrifuged for 5 min at 14,000 rpm. The pellet was collected and cleaned with ethanol, and the supernatant was removed in order to crystallize the SF and remove any free medicines. After further centrifugation at 14,000 rpm for 5 min, the supernatant was collected. The residual particle was resuspended in double-distilled water and centrifuged twice at 14000 rpm to eliminate any remaining ethanol. The nanoparticles were resuspended in 1 ml of 7.4 pH phosphate buffer solution (PBS) and used for additional investigation [14].

Solvent change method

Using a sample pipette at room temperature, SF solution containing 5.0% by weight was quickly added to at least 70% (v/v) of the final mixed volume of the water-miscible organic solvent acetone. The SF-NPs were water-insoluble and dissipated slowly due to NP accumulation in the mixture of water and organic solvent. The mixture was repeatedly centrifuged at 12,000 rpm to separate the SF-NPs residues from the solvent, and then these particles were collected and purified. The nanoparticle residues in water dispersed uniformly in water or PBS media after being subjected to a supersonic treatment for 1 to 5 min. The obtained liquid or lyophilized SF-NPs were used in additional experiments [15].

Analysis of particle size, zeta potential, polydispersity index (PDI), and entrapment efficiency (EE)

The average particle size, zeta potential, and PDI were determined using the Zeta-sizer (Nano ZS, Malvern Instruments, UK) and the dynamic light scattering (DLS) technique. The total charge that a particle picks up in a certain medium is known as its zeta potential. This method included passing a voltage across two electrodes located at both ends of a cell bearing the nanoparticles. Milli-Q water was used to dilute samples from the prepared suspensions before they were put in measurement cells for analysis [16]. EE was assessed using the indirect method. In this method, the formulated SF-ANS-NPs-1 was centrifuged at 12,000 rpm for a period of 15 min. Using a UV/visible spectrophotometer with a maximum wavelength of 262 nm, the amount of ANS that was not trapped in the precipitate was calculated. To reduce handling errors, the entire analysis was conducted three times [17, 18].

$$EE = \frac{\text{Amount of drug added in the formulation} - \text{Amount of untrapped drug in the formulation}}{\text{Amount of drug added in the formulation}} \times 100$$

Fourier transform infrared spectroscopy analysis (FT-IR)

ANS's compatibility with the excipients used in the formulation of NPs were assessed using FT-IR spectrophotometer (Shimadzu, Japan). Optimal SF-ANS-NPs-1 spectra were obtained in the 4000-400 cm^{-1} region, along with spectra of pure ANS, SF, and physical combinations of the formulation [19].

Determination of *in vitro* release

The SF-ANS-NPs-1 was dissolved in 1.0 ml of PBS (pH = 7.4), equivalent to 1 mg, and sealed cellulose dialysis tubing (Carolina, Burlington, NC, USA) with a cut-off of 12,000–14,000 Da was used. After that, 19.0 ml of release media was added to a screw-cap container containing dialysis tubing, which was then stored in a water bath shaker (GFL 1083; GFL, Burgwedel, Germany) set to medium speed and 37 °C. Aliquots of 2.0 ml were taken out and immediately replaced with the same volume of the fresh-release medium at various intervals. Using a UV-1900, the levels of medication emitted were measured at the peak of 262 nm (Shimadzu, Japan). The results presented are, in practice, the mean and standard deviation of triplicates (Mean SD) using the prescribed methodology [20, 21].

Release kinetics study

Mathematical equations such as Higuchi's diffusion equation ($Q = Kt^{1/2}$), Korsmeyer-Peppas equation ($Mt/M = Kt^n$), and zero-order (percent release vs. t) and first-order kinetics (log percent release vs. t) were used to model the drug release from the optimized SF-ANS-NPs-1 formulation. In the equation, Mt/M is the fraction of the

drug released at time t , k is the kinetic constant, and n is the diffusional exponent [22, 23].

Differential scanning calorimetry studies (DSC)

Using the DSC-60 equipment, differential scanning calorimetry was used to examine the phase behavior of drug-loaded particles. The instrument was made up of a thermal analyzer (TA 60), a flow controller (FCL 60), a calorimeter (DSC 60), and operational software (TA 60) from the Kyoto, Japan-based Shimadzu firm. Pure drug and SF-ANS-NPs-1 samples weighing 2–10 mg each were put in aluminum pans and crimped before being heated under nitrogen flow at a rate of 5 °C/min from 25 °C to 250 °C. As a benchmark, a pan made of aluminum having the same amount of indium was employed. Both pure drugs and nanoparticles had their heat flow assessed as a function of temperature [24].

Powder X-ray diffraction analysis (PXRD)

By using a Bruker (Advance D8) powder diffractometer, PXRD analysis was performed (Karlsruhe, Germany). The samples to be analyzed were spread out on an amorphous silica hold, a low background sample holder, and fixed to this sample stage in a goniometer. The geometry of the instrument is set to B-B. To 40 mV and 40 mA, respectively, the voltage and current are adjusted. Data extraction was done after copper radiation was used to acquire scans from 2 to 50° with a step size of 0.03°, and a count time of 0.5 s at 25 °C [24].

Field emission scanning electron microscopy (FESEM)

The surface structure of the optimized SF-ANS-NPs-1 was evaluated using a field emission scanning electron microscope (FESEM, Carl Zeiss Sigma-03-81, Oxford Instruments, EDS). Overnight, a droplet of nanoparticle solution was applied to a copper layer, fitted over the tip of the sample, and allowed to dry. Each sample was coated with platinum before investigation [25, 26].

High-resolution transmission electron microscopy (HR-TEM)

Using transmission electron microscopy, the morphology of nanoparticles was studied. To visualize NPs, a (JEM-2100 electron microscope; JEOL, Tokyo, Japan) was used. The SF-ANS-NPs-1 formation was analyzed using the negative staining TEM technique. A 50 μl sample of the nanoparticle formulation was collected and coated in parafilm. Samples were dried on the carbon-coated grid and stained negatively with a phospho-tungstic acid aqueous solution. The sample was investigated under a microscope at 10 to 100 k fold expansion after drying at a 100 kV accelerating voltage [21].

Stability study of SF-ANS-NPs-1

The optimized SF-ANS NPs-1 were put in 5 ml sample vials and subjected to accelerated stability testing as per ICH recommendations. The bottles were kept at 5 °C in the refrigerator for three months and at 25 °C and 75±5% RH for an accelerated time. At predetermined time intervals and frequencies, the physical aspect, size, zeta potential, particle distribution, and percentage of EE of nanoparticles were analyzed [27].

Preparation of *in situ* gel formulation with pluronic F-127

Thermo-responsive *in situ* gel was prepared according to the cold method. Pluronic F-127 (18% w/v) is weighed out and added gradually (over the course of 2 or 3 min) to 20 ml of cold water (5–10 °C) in a 100 ml beaker with a magnetic stirring bead, ensuring gentle mixing. This enables each flake to become hydrated on the surface and increases the rate of solution, whereas rapid addition of all the pluronic F-127 to the water results in the formation of a large ball requiring many hours to dissolve. The container was placed in an ice bath for about 4 hr and mixed slowly until the pluronic F-127 had completely dissolved. When the solution is complete and the formulation warms, the *in situ* injectable gel is formulated [28].

Evaluation studies of *in situ* gel

Appearance and clarity

For pharmaceutical solutions that are administered parenterally, the visual appearance of the formulation in terms of clarity is crucial. Particulate matter can cause tissue discomfort or potentially be

toxic, in addition to having an impact on patient compliance. Both formulations were visually examined for clarity in a bright environment with a black-and-white background [29].

Sol-gel transition temperature

The sol-gel transition temperature is the point at which, when maintained in a sample tube at a particular temperature and then heated at a specific pace, the phase change of the sol meniscus first becomes apparent. Gel should not move when the tube is bent, which is an indication that gel has developed. The gel-forming solution was transferred to a tiny, clear beaker, which was then positioned in a temperature-controlled water bath. The beaker was filled with a magnetic bead and a thermometer, and the solution was heated progressively while continuously stirring at 30 rpm. The temperature on the thermometer submerged in the solution was identified as the gelation temperature when the magnetic bar stopped moving due to gelation [30].

Rheological behavior studies

The viscosity of SF-ANS-NPs-1 loaded *in situ* injectable was measured using Brookfield viscometer (model DV-II+Pro), Engineering Laboratories, Middleboro, MA 02346) 20 ml of SF-ANS-NPs loaded *in situ* injectable was taken into a beaker. The spindle nos. F 96 at 10, 50 in 10, 50, and 100 rpm at 24-25 °C. The spindles were immersed in the test fluid. Viscosity values were recorded [31].

Determination of pH

A digital pH meter was used to measure the pH level of the optimized gel formulation (LMPH-10, LABMAN). After 5 min of immersion, the pH meter probe was removed, and readings were collected. An average of three samples were used to take the readings [32].

Syringability study

The ability of the prepared formulation to flow easily through a syringe of the 21-gauge needle was assessed. Briefly, 1 ml of the cold SF-ANS-NPs-1 incorporated *in situ* injectable gel formulation (4 °C) and at room temperature (25 °C) was filled in a 21-gauge needle syringe, and the capacity to flow under standard handling pressure was evaluated [33].

In vitro drug release study for *in situ* gel

Franz diffusion apparatus and PBS (pH=7.4) as a dissolution media were used to conduct release investigations of SF-ANS-NPs-1

incorporated *in situ* gel. The pre-hydrated membrane was mounted between the matched receptor and doner compartment 2 ml of gel was taken into the doner compartment. All openings, including the doner top and receptor arm, were occluded with parafilm to prevent evaporation. The rotational speed was held constant at 200–250 rpm while the temperature was kept at 37±0.5 °C. The samples (1-2 ml) were withdrawn using a glass syringe at various time intervals and analyzed spectrophotometrically at 262 nm. A fresh medium of the same volume was reintroduced into the receptor. The reported results are triplicate averages and are presented as Mean SD [34].

Kinetics of drug release of *in situ* gel

To determine the kinetics of drug release, the dissolution profile of SF-ANS-NPs-1 loaded *in situ* gel was fitted to kinetic models including zero order, first order, Higuchi, Korsmeyer, and peppas. The process of drug release from the formulation is shown by the diffusion exponent n. The n value is employed to comprehend various release processes, leading to values for a slab of n<0.5 for the fickian diffusion mechanism and 0.5<n<1.0 for non-fickian transport [35].

Accelerated stability study of *in situ* gel

The *in situ* gel composition was put in a glass bottle with a cap to close it. It had a secure seal. The stability study was conducted following ICH guidelines, at 25±2 °C/75±5% RH for room temperature and 4 °C±2 °C for 90 d. Periodically (30, 60, and 90 d), samples were taken out and examined for visual quality, pH, viscosity, and sol-gel transition [36].

RESULTS AND DISCUSSION

Particle size, zeta potential, PDI, and EE analysis

characterize the particles. The size analysis of both batches of nanoparticles was conducted in triplicate. Whereas SF-ANS-NPs-2 was discovered to be larger than 400 nm, SF-ANS-NPs-1 was discovered to be present in the size range below 200 nm. Similarly, the PDI showed a distribution that was relatively uniform, ranging from 0.10±01 to 0.80±06 for both formulation batches. Zeta potential measurements for the ANS-NPs were 27±2.14 and -1.88±3 (table 1). The medication was effectively trapped, according to entrapment studies, showing that they are effectively neutral in charge and can be distributed in a physiological pH media. This investigation has led to the development of a successful method for formulating and optimizing the suitable injectable size of SF-ANS-NPs-1 [37].

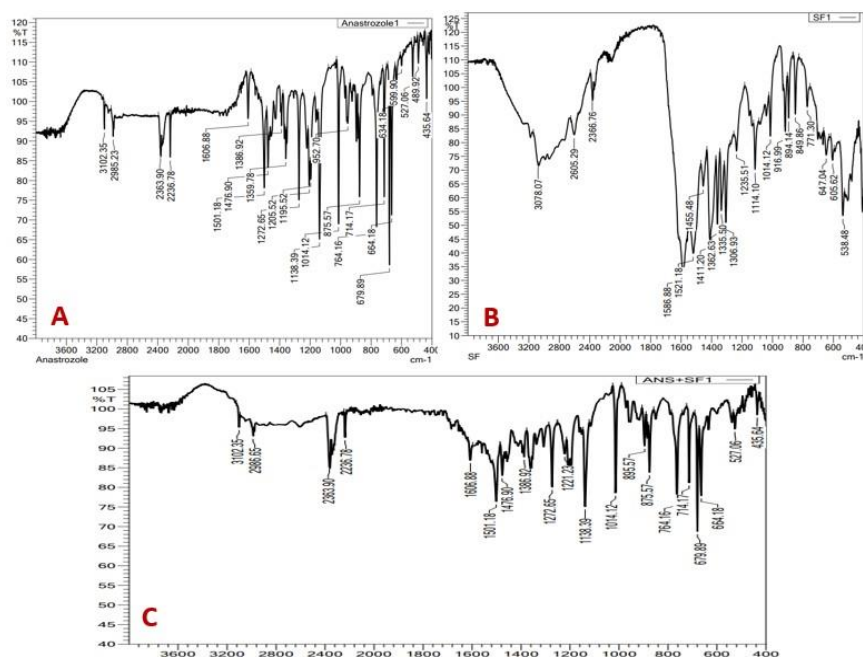


Fig. 1: FT-IR spectrums of (A) pure ANS, (B) silk fibroin, (C) SF-ANS-NPs-1

Table 1: Particle size, zeta potential, PDI, and % EE of formulated nanoparticles with solvent precipitation (Method 1, SF-ANS-NPs-1) and solvent change method (Method 2, SF-ANS-NPs-2)

Method	Formulation code	Particle size (nm)	Zeta potential (mV)	PDI	EE (%)
Solvent precipitation	SF-ANS-NPs-1	181.70±1.3	27.09±2.14	0.10±01	89±2.21
Solvent change	SF-ANS-NPs-2	421.60±2.0	-1.88±3.41	0.70±06	78±1.91

mean±SD (n = 3)

FT-IR analysis

Fig. 1 depicts the FT-IR spectra of pure ANS, the polymers utilized in the formulation, and the optimized formulation SF-ANS-NPs-1. The spectral analysis revealed that the peaks of the chosen optimal formulation and the pure medication did not differ noticeably. As a result, no particular

interaction between the medication and the formulation's polymers was seen. Substantial O=C=O, C-O, Medium C-H, and Weak C-N stretch absorption peaks were seen in the infrared ANS spectra at 2363.90, 1138.39, 3102.35, and 2236.78, correspondingly. There are no interactions between ANS and the investigated excipients because the identical bands are present in SF-ANS-NPs-1 [38].

Table 2: FT-IR characteristic peaks of pure ANS, SF, and SF-ANS-NPs-1

Sample compounds	O=C=O (cm ⁻¹)	C-O (cm ⁻¹)	C-H (cm ⁻¹)	C≡N (cm ⁻¹)	N-O (cm ⁻¹)
ANS	2363.90	1138.39	3102.35	2236.78	-
SF	2366.76	1114.10	3078.07	-	1586.88
SF-ANS-NPs-1	2358	1084	3310	-	-

In vitro drug release of SF-ANS-NP-1

According to the results presented, the use of nanoscale drug formulations has been found to improve the release profile of the drug in investigations, as evidenced by the optimized SF-ANS-NPs-1, which showed more than 94.15% drug release in 168 h displayed in

fig. 2. A burst release phase follows a continuous release phase on the initial day. Diffusion of the aqueous dissolution medium into the matrix, followed by drug diffusion into the dissolution media through the pores, enables the drug to dissolve. The retention period of ANS release was significantly improved by using the appropriate concentration of SF [39, 40].

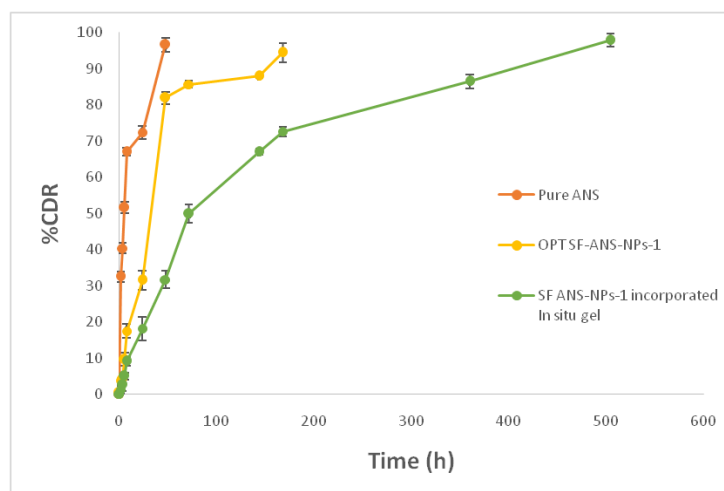
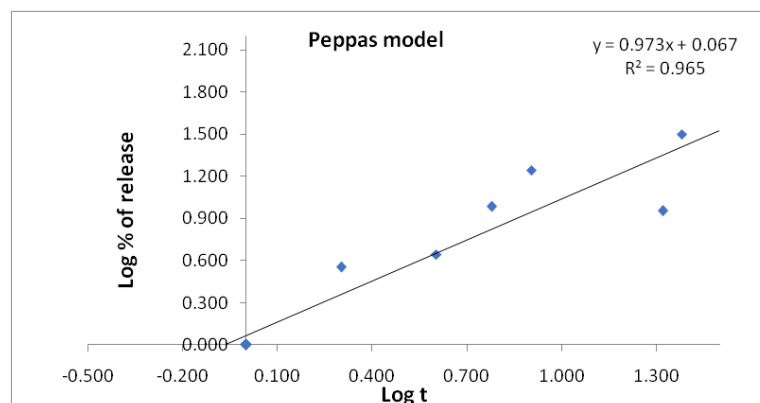
**Fig. 2: Release profile of pure ANS, optimized SF-ANS-NPs-1 and SF-ANS-NP loaded *in situ* gel, (mean±SD, n = 3)****Fig. 3: Plot of log time vs. log % drug release (Peppas's model)**

Table 3: Kinetic data table of SF-ANS-NPs-1

Formulation code	Zero-order	First order	Korsmeyer peppa's model	Higuchi model	Best fit model
SF-ANS-NPs-1	0.8546	0.8909	0.9651	0.9091	Peppa's model

Drug release kinetic studies for SF-ANS-NPs-1

The Korsmeyer Peppa's model plot of the SF-ANS-NPs-1 was found to be linear with the R^2 value of 0.9651, respectively (fig. 3 and table 3). The n -value $0.5 < n < 1.0$ for SF-ANS-NPs-1 suggests the anomalous (Non-Fickian) transport mechanism [41].

DSC analysis

Fig. 4 displays the DSC thermograms of ANS, SF, physical mixture, and SF-ANS-NPs-1. The endothermic peak for pure anastrozole, which corresponds to its melting point at 88.94 °C and further supports its crystalline form, was prominent and well-defined. In

contrast, the physical combination and anastrozole-loaded optimized nanoparticles showed no melting endotherm, suggesting that anastrozole may be transformed into its amorphous state. According to the DSC study results for drug-loaded nanoparticles, the strength of endothermic peaks was lessened and distinct, with a different melting transition than that seen with the pure drug, leading to the production of a new amorphous phase. The SF-ANS-NPs-1 demonstrated that the drug existed evenly and was distributed at the molecular level in a disorganized crystalline structure, which led to its improved solubility, in addition to the new amorphous state. These findings together show that the drug's melting peak is altered as a result of nanoparticle formation [37, 42].

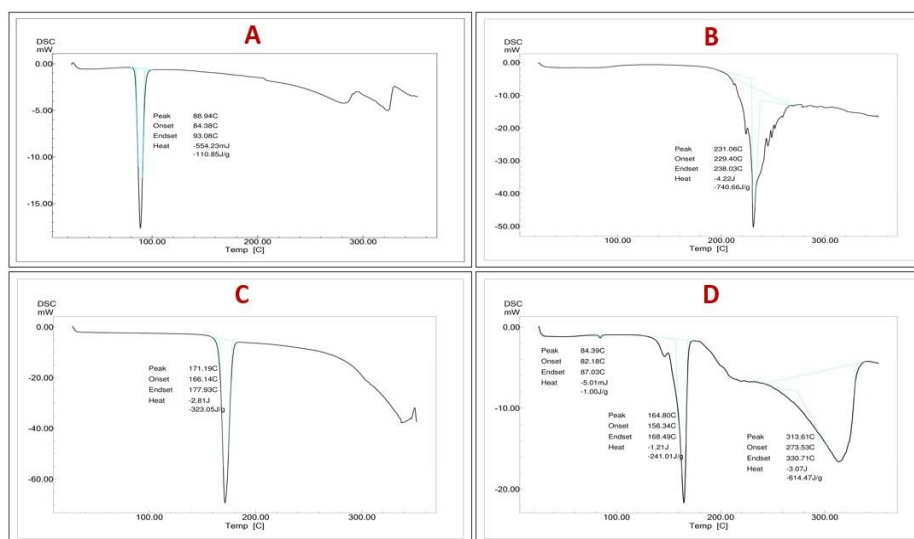


Fig. 4: DSC curves for A. ANS, B. silk fibroin, C. physical mixture, and D. SF-ANS-NPs-1

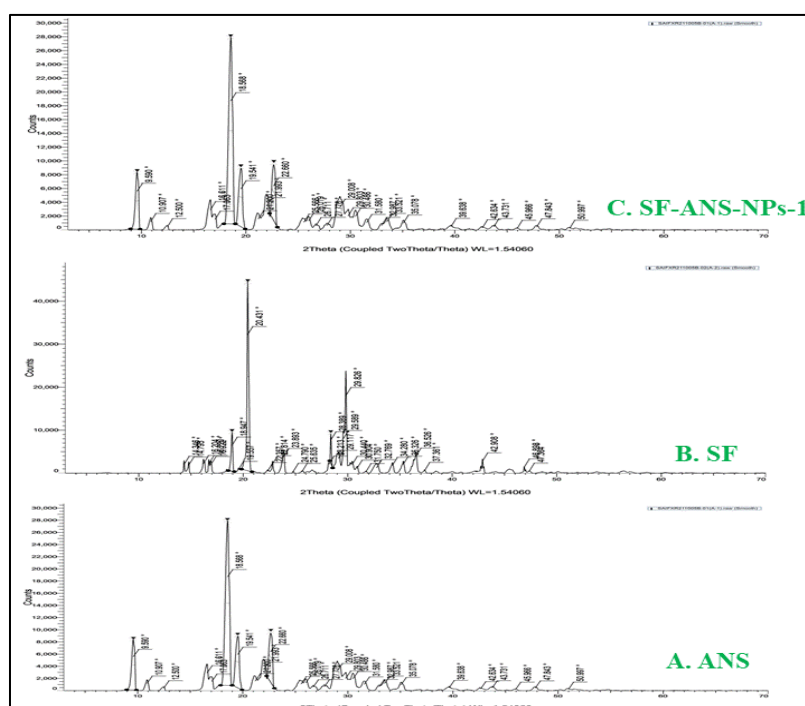


Fig. 5: X-ray diffractograms of (A) ANS, (B) SF, and (C) SF-ANS-NPs-1

X-ray diffraction studies

Pure ANS has well-defined, sharp diffraction peaks in its X-ray diffraction pattern. When seen from a 2θ angle, it was discovered that the intensity count of 18.56 was in the 20001-intensity count, with a 100% relative intensity. The distinctive pattern of amorphous silk material, known as a wide peak at $2\theta = 20^\circ$, was seen in SF. An intensity count of 11291.0 with 100% relative intensity at a 2θ angle of 20.362 was shown in the X-ray diffraction patterns for SF-ANS-NPs-1. When compared to the pure drug, the diffractograms in fig. 5 demonstrate a variety of alterations in peak positions and a noticeably different diffraction pattern. As compared to pure drug and SF, the relative intensity in 2θ angle value for the nanoparticles was found to be different, showing molecular level drug distribution in the polymer structure [43].

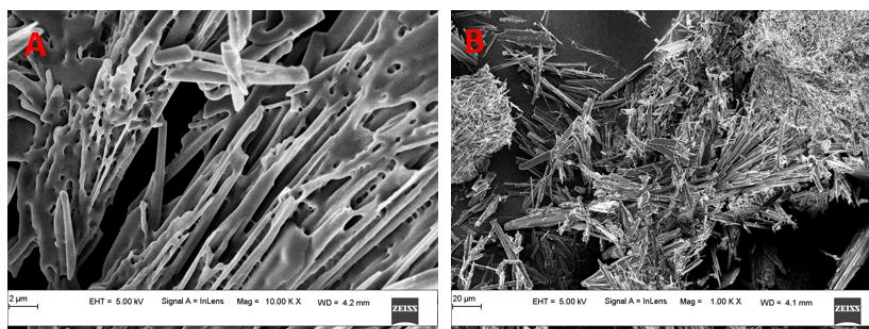


Fig. 6: FE SEM images of SF-ANS-NPs-1 in A. 10.00 K X and B. 1.00 K X magnification

HR-TEM analysis

The shape and size distribution of the SF-ANS-NPs-1 were observed using HR-TEM analysis shown in fig. 7. They were found to be well-dispersed, spherical, and seen present in distinct particles. The particle size of the NPs were also determined using TEM, and the results were consistent with those obtained using DLS analysis [44].

Stability study for optimized SF-ANS-NPs-1 formulation

When stored in accordance with ICH guidelines under accelerated conditions of $25 \pm 2^\circ\text{C}/75 \pm 5\% \text{RH}$ and at refrigerating conditions ($4^\circ\text{C} \pm 2^\circ\text{C}$) for a duration of three months, SF-ANS-NPs-1 did not exhibit any physical alterations. Zeta-potential, PDI, and % EE (less than 5%)

Surface morphology analysis

The surface morphology of optimized SF-ANS-NPs-1 is depicted in fig. 6. Images with great resolution were taken using FE-SEM. Images revealed that nanoparticles had uniform size, were dispersed in a straight crystalline structure with a smooth surface, and were separate particles. The distribution of their sizes was constrained, and they were orientated closely together. Using the proper sonication intensity throughout the formulation process may be able to achieve this. Furthermore, the results of the FE-SEM analysis demonstrate that a matrix structure was formed as a consequence of the interaction between the polymer and the drug. This finding demonstrates that drug molecules were extensively distributed in polymeric structures, which can result in the formation of nanoparticles [43].

at the predetermined time intervals similarly showed no discernible change. Particle size mildly grew larger. Nonetheless, it was determined that the overall provided data was within accepted limits (table 4). This shows that the optimized SF-ANS-NPs-1 is highly stable and effective by nature across a three-month period [45].

Physical evaluation parameters

The prepared SF-ANS-NPs-1 loaded *in situ* gel was translucent to clear dispersion and slightly brownish in color, which is because of the addition of SF. The haziness observed during preparation was due to the precipitation of pluronic F-127. At reduced temperature was found to disappear, and the clarity was regained after overnight standing [46].

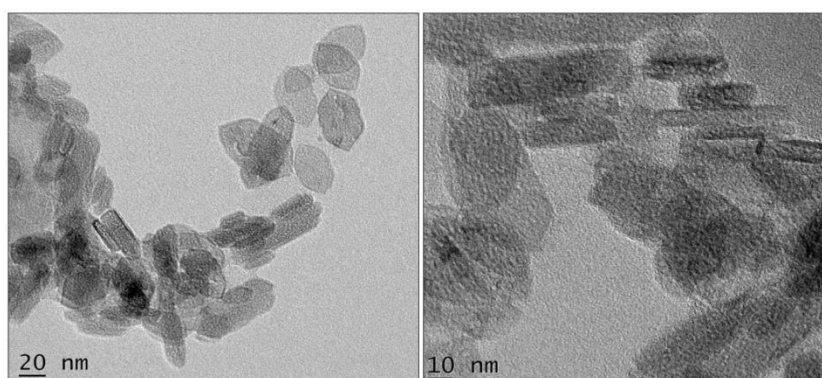


Fig. 7: HR-TEM analysis of SF-ANS-NPs-1 formulation

Sol-gel temperature

The data for assessing the thermos-responsive *in situ* gel's gelation temperature was found to be $37 \pm 0.5^\circ\text{C}$ shown in fig. 8. Gelation at temperatures of $35\text{--}37^\circ\text{C}$ is considered to be optimal for the development of a thermosensitive *in situ* gelling solution for implantation since temperatures below 30°C would lead to gelation

at ambient temperature and problems with manufacture, processing, and delivery. On the other side, the formulation would remain fluid after administration if the gelation temperature was greater than 37°C . The inclusion of pluronic F-127 solutions raises the formulation's gelation temperature, bringing it closer to the physiological temperature range. When the concentration in the formulation increased, the gelation temperature showed a modest rise.

Table 4: Particle size, zeta potential, PDI, and % EE of SF-ANS-NPs-1 at 4±2 °C and 25±2 °C/75±5% RH

At room temperature (25 °C)				At refrigerating conditions (4 °C)				
Time (months)	Particle size (nm)	Zeta potential (mV)	PDI	EE (%)	Particle size (nm)	Zeta potential (mV)	PDI	EE (%)
1	185.50±1.4	2.91±2.1	0.57±0.06	86.91±1.5	188.50±2.4	2.11±2.1	0.47±0.06	88.41±2.5
2	181.11±2.11	3.11±3.2	0.57±0.09	88.82±0.5	181.11±2.11	2.11±3.2	0.47±0.09	87.52±0.9
3	176.97±1.88	3.78±2.4	0.56±0.11	88.88±0.9	176.97±1.88	3.78±2.2	0.46±0.11	85.58±1.9

Results are expressed as mean±SD (n=3)

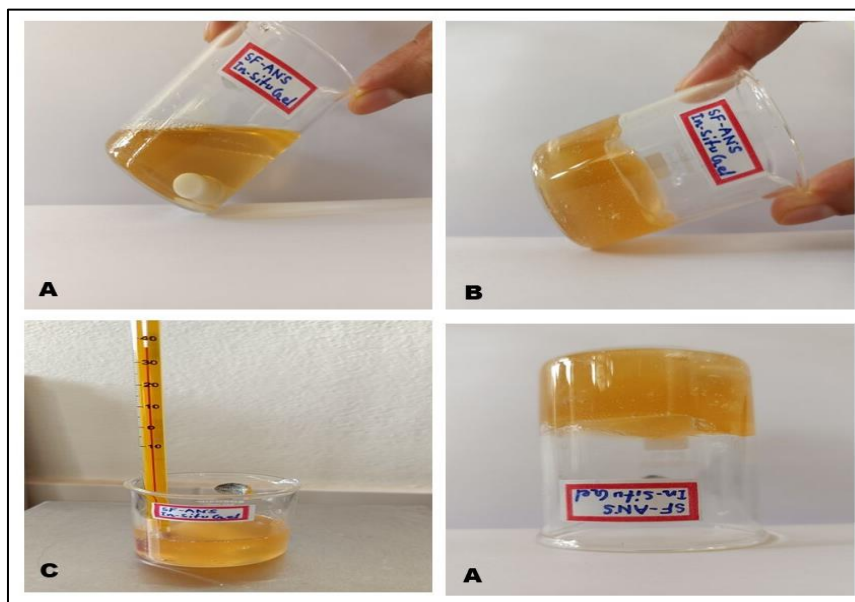


Fig. 8: SF-ANS-NPs-1 loaded *in situ* gel formulation A. at room temperature and B. after temperature increases (≥ 37 °C). C. Noted temperature at gelling point and D. inverted beaker after gelation

Rheological behavior studies

Considering that the refrigerated formulations will only be delivered after being brought to room temperature, low dynamic viscosity at 20 to 25 °C is needed to inject the formulation freely. The SF-ANS-NPs-1 loaded *in situ* gel exhibited quite low viscosity of 9.37 ± 1.2 mPa·s at room temperature, which indicated its suitability as an injectable *in situ* gel formulation [24].

pH determination

During the process of cancer progression, the tumor microenvironment causes tumor heterogeneity. Acidic conditions and hypoxia are well-known to be significant elements of the tumor microenvironment. SF-ANS-NP-1 loaded *in situ* gel showed an acidic pH (table 5) which is an ideal characteristic for anti-tumor formulations.

Table 5: pH at different temperature conditions

S. No.	Temperature	pH of gel*
1.	4 °C	6.8±0.09
2.	25 °C	6.8±0.1
3.	After gelation	6.7±0.09

*Results are expressed as mean±SD (n=3)

Syringeability study

The developed SF-ANS-NP loaded *in situ* gel formulations were easily syringeable through a 21-gauge needle at room temperature [47].

In vitro drug release for SF-ANS-NP-1 loaded *in situ* gel

The *in-situ* gelling formulation could enable a sustained and regulated release of the drug, according to the *in vitro* release profile. By the end of the 504th hour (21 D), the *in-situ* gel showed a total drug release of 98.11% (fig. 2). The formulas only released a small preliminary burst. Due to the drug's slow diffusion through the matrix material, the subsequent stage of the release can be extended. The initial burst release can be attributed to the *in-situ* gelling

mechanism, which was in sol form at ambient temperature but transformed into a gel due to increased heat when the *in-situ* gel formulation was introduced to physiological temperature. However, the outcomes undeniably demonstrate that the gels can hold the drug for a long time and that early drug release will not happen [20].

Drug release kinetic studies for SF-ANS-NPs-1 *in situ* gel

The gel formulation was determined to follow first-order model kinetics from the release kinetics data, based on the highest coefficient of determination value (R^2) = 0.9721, which is close to unity (fig. 9 and table 6). The n-value of $0.5 < n < 1.0$ for the SF-ANS-NP-1 incorporated *in situ* gel, when plotted using the Korsmeyer-Peppas method, indicates anomalous (non-Fickian) transport and is shown as an extended-release mechanism [48].

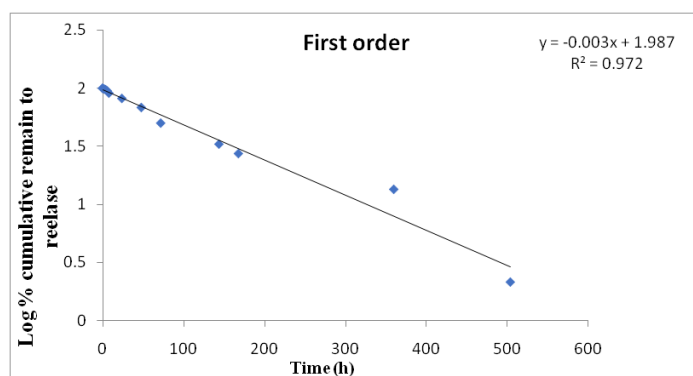


Fig. 9: Plot of Time vs. log % drug remaining (First order model)

Table 6: Kinetic data of silk fibroin-anastrozole nanoparticle incorporated *in situ* gel

Formulation code	Zero-order (R ²)	First order (R ²)	Korsmeyer peppas's model (R ²)	Higuchi model (R ²)	Best fit model (R ²)
SF-ANS-NP-1 <i>In situ</i> gel	0.8601	0.9721	0.9274	0.9652	First order

Table 7: Visual appearance, pH, viscosity (mPa·s), sol-gel transition temperature, and % CDR of optimized SF-ANS-NP-1 loaded *in situ* gel formulation at 25±2 °C/60±5% RH and at 4±2 °C temperature

Physical parameters	At 25±2 °C Temperature			At 4±2 °C temperature		
	30 th Day	60 th day	90 th day	30 th Day	60 th day	90 th day
Visual appearance	Clear and yellowish in color					
pH	6.7±0.09	6.8±0.02	6.7±0.04	6.8±0.08	6.9±0.04	6.8±0.07
Viscosity mPa·s	10.40±0.16	12.52±0.09	11.57±0.01	09.20±0.36	12.12±0.05	10.67±0.04
Sol-gel transition temp (°C)	36±0.10	35±0.42	37±0.51	35±0.30	36±0.12	37±0.81
%CDR at 504 th h	97.06±2.06	95.96±1.22	95.09±2.12	96.05±1.04	96.16±2.50	94.14±1.09

Results are expressed as mean±SD (n=3)

Stability study of SF-ANS-NP-1 loaded *in situ* gel

No significant changes in visual appearance, pH, viscosity, sol-gel transition, and % CDR were observed during the 3-month stability study shown in table 7. Hence the formulation can be found stable for at least a period of 3 mo [49].

CONCLUSION

A biodegradable polymer SF was used to successfully develop ANS NPs by solvent change and solvent precipitation methods. The ANS was well-encapsulated in both formulations, with particles ranging in size from 181.70 to 421.60 nm. *In situ* gel formulation incorporating SF-ANS-NPs-1 showed prolonged *in vitro* drug release and desired stability. The current study effort has shown how to translate a theoretical concept into a practical application and solve problems step-by-step. NPs based on SF would enable more prolonged therapy for breast cancer. It can dramatically increase patient compliance, and prolong the duration of that therapy will have an effect. However, there is a lot that could be done to treat and maybe prevent advanced cancer by starting cancer prevention at the earliest practical stage. In conclusion, it can be said that instead of using new therapeutic molecules, established drugs could be repurposed to develop stable and effective dosage forms for long-term BC treatment.

LIST OF ABBREVIATIONS

Abbreviation	Definition
BC	Breast cancer
ER.	Estrogen receptor
ANS	Anastrozole
NP	Nanoparticle
SF	Silk fibroin
PDI	polydispersity index
EE.	entrapment efficiency
DLS	dynamic light scattering
FT-IR	Fourier-transform infrared spectroscopy
PBS	Phosphate buffer solution
SD	Standard Deviation

DSC	Differential scanning calorimetry
PXRD	Powder X-ray diffraction
FESEM	Field emission scanning electron microscopy
HR-TEM	High-resolution transmission electron microscopy
CDR	Cumulative drug release

ACKNOWLEDGEMENT

Researchers are thankful to Sericare, and Cipla, Bangalore, for providing silk fibroin and anastrozole gift samples used in the study and DST-SAIF Cochin for sample analysis. The authors would like to thank Yenepoya Pharmacy College and Research Centre, Yenepoya (Deemed to be University), for the provision of laboratory facilities to perform the experimental works.

FUNDING

No specific grant was given to this research by any funding organization in the public, private, or non-profit sectors.

AUTHORS CONTRIBUTIONS

Mrs. Arfa Nasrine made contributions to the idea, the method, the validation, the research, and the writing of the original manuscript. Dr. Mohammed Gulzar Ahmed made a contribution to the investigation and manuscript evaluation. Reviewing and editing by Ms. Soumya Narayan.

CONFLICT OF INTERESTS

No conflict of interest should exist regarding the authorship of this research study, according to the authors.

REFERENCES

- Verma V, Hiremath RN, Basra SS, Kulkarni PC, Ghodke S. Early surgical outcomes of operable breast cancer patients based on molecular subtyping—a single-centre study. *Asian J Pharm Clin Res.* 2023;16:67-70. doi: 10.22159/ajpcr.2023.v16i3.46564.
- Early Breast Cancer Trialists' Collaborative Group (EBCTCG), Davies C, Godwin J, Gray R, Clarke M, Cutter D. Relevance of breast cancer hormone receptors and other factors to the

- efficacy of adjuvant tamoxifen: patient-level meta-analysis of randomised trials. *Lancet*. 2011;378(9793):771-84. doi: 10.1016/S0140-6736(11)60993-8, PMID 21802721.
3. Davies C, Pan H, Godwin J, Gray R, Arriagada R, Raina V. Long-term effects of continuing adjuvant tamoxifen to 10 years versus stopping at 5 y after diagnosis of oestrogen receptor-positive breast cancer: ATLAS, a randomised trial. *Lancet*. 2013;381(9869):805-16. doi: 10.1016/S0140-6736(12)61963-1, PMID 23219286.
 4. Neuner JM, Kamaraju S, Charlson JA, Wozniak EM, Smith EC, Biggers A. The introduction of generic aromatase inhibitors and treatment adherence among medicare D enrollees. *J Natl Cancer Inst*. 2015;107(8):1-7. doi: 10.1093/jnci/djv130, PMID 25971298.
 5. Rukminingsih F, Andayani TM, Rahmawati F, Widayati K. Health-related quality of life in early breast cancer patients with hormone responsive. *Int J Pharm Pharm Sci*. 2018;10(12):47. doi: 10.22159/ijpps.2018v10i12.29648.
 6. Russo J, Russo IH. The role of estrogen in the initiation of breast cancer. *J Steroid Biochem Mol Biol*. 2006;102(1-5):89-96. doi: 10.1016/j.jsmb.2006.09.004, PMID 17113977.
 7. Kunde SS, Wairkar S. Targeted delivery of albumin nanoparticles for breast cancer: a review. *Colloids Surf B Biointerfaces*. 2022;213:112422. doi: 10.1016/j.colsurfb.2022.112422, PMID 35231688.
 8. Gajbhiye SA, Patil MP. Solid lipid nanoparticles: a review on different techniques and approaches to treat breast cancer. *Int J App Pharm*. 2023;15:52-62. doi: 10.22159/ijap.2023v15i2.46970.
 9. Correa S, Grosskopf AK, Lopez Hernandez H, Chan D, Yu AC, Stapleton LM. Translational applications of hydrogels. *Chem Rev*. 2021;121(18):11385-457. doi: 10.1021/acs.chemrev.0c01177, PMID 33938724.
 10. Pandey M, Choudhury H, Binti Abd Aziz ABA, Bhattamisra SK, Gorain B, Su JST. Potential of stimuli-responsive in situ gel system for sustained ocular drug delivery: recent progress and contemporary research. *Polymers (Basel)*. 2021;13(8). doi: 10.3390/polym13081340, PMID 33923900.
 11. Zuluaga Velez A, Quintero Martinez A, Orozco LM, Sepulveda Arias JC. Silk fibroin nanocomposites as tissue engineering scaffolds—a systematic review. *Biomed Pharmacother*. 2021;141. doi: 10.1016/j.biopha.2021.111924.
 12. Kundu B, Rajkhowa R, Kundu SC, Wang X. Silk fibroin biomaterials for tissue regenerations. *Adv Drug Deliv Rev*. 2013;65(4):457-70. doi: 10.1016/j.addr.2012.09.043, PMID 23137786.
 13. Zhao Z, Li Y, Xie MB. Silk fibroin-based nanoparticles for drug delivery. *Int J Mol Sci*. 2015;16(3):4880-903. doi: 10.3390/ijms16034880, PMID 25749470.
 14. Mishra D, Iyyanki TS, Hubenak JR. Silk fibroin nanoparticles and cancer therapy. *Nanotechnol cancer*. Elsevier Inc; 2017.
 15. Zhang YQ, Shen W, Xiang RL, Zhuge L, Gao W, Wang W. Formation of silk fibroin nanoparticles in water-miscible organic solvent and their characterization. *J Nanopart Res*. 2007;9(5):885-900. doi: 10.1007/s11051-006-9162-x.
 16. Shavi GV, Nayak UY, Maliyakkal N, Deshpande PB, Raghavendra R, Kumar AR. Nanomedicine of anastrozole for breast cancer: physicochemical evaluation, *in vitro* cytotoxicity on BT-549 and MCF-7 cell lines and preclinical study on rat model. *Life Sci*. 2015;141:143-55. doi: 10.1016/j.lfs.2015.09.021, PMID 26423561.
 17. Labib S, Nasr M, Nasr M. Formulation and evaluation of atorvastatin calcium nanocrystals containing p-glycoprotein inhibitors for enhancing oral delivery. *Int J Curr Pharm Sci*. 2021;13(3):19-23. doi: 10.22159/ijcpr.2021v13i3.42087.
 18. Nasrine A, Gulzar Ahmed M, Narayana S. Silk fibroin-anastrozole loaded prolonged-release biodegradable nanomedicine: a promising drug delivery system for breast cancer therapy. *Mater Today Proc*. 2022;68:56-65. doi: 10.1016/j.matpr.2022.06.101.
 19. Sitrarasi R, Nallal VUM, Razia M, Chung WJ, Shim J, Chandrasekaran M. Inhibition of multi-drug resistant microbial pathogens using an eco-friendly root extract of *Furcraea foetida* mediated silver nanoparticles. *J King Saud Univ Sci*. 2022;34(2):101794. doi: 10.1016/j.jksus.2021.101794.
 20. Cao Z, Tang X, Zhang Y, Yin T, Gou J, Wang Y. Novel injectable progesterone-loaded nanoparticles embedded in SAIB-PLGA in situ depot system for sustained drug release. *Int J Pharm*. 2021;607:121021. doi: 10.1016/j.ijpharm.2021.121021, PMID 34416333.
 21. Rattanawongwiboon T, Soontaranon S, Hemvichian K, Lertsarawat P, Laksee S, Picha R. Study on particle size and size distribution of gold nanoparticles by TEM and SAXS. *Radiat Phys Chem*. 2022;191:109842. doi: 10.1016/j.radphyschem.2021.109842.
 22. El-assaal MI, Samuel D. Optimization of rivastigmine chitosan nanoparticles for neurodegenerative Alzheimer; *in vitro* and *in vivo* characterizations. *Int J Pharm Pharm Sci*. 2022;14:17-27. doi: 10.22159/ijpps.2022v14i1.43145.
 23. Bai X, Smith ZL, Wang Y, Butterworth S, Tirella A. Sustained drug release from smart nanoparticles in cancer therapy: a comprehensive review. *Micromachines*. 2022;13(10):1-54. doi: 10.3390/mi13101623, PMID 36295976.
 24. Shavi GV, Nayak UY, Reddy MS, Ginjupalli K, Deshpande PB, Averineni RK. A novel long-acting biodegradable depot formulation of anastrozole for breast cancer therapy. *Mater Sci Eng C Mater Biol Appl*. 2017;75:535-44. doi: 10.1016/j.msec.2017.02.063, PMID 28415496.
 25. Zhang Z, Feng SS. The drug encapsulation efficiency, *in vitro* drug release, cellular uptake and cytotoxicity of paclitaxel-loaded poly(lactide)-tocopherol polyethylene glycol succinate nanoparticles. *Biomaterials*. 2006;27(21):4025-33. doi: 10.1016/j.biomaterials.2006.03.006, PMID 16564085.
 26. Dong Y, Feng SS. Poly(D,L-lactide-co-glycolide) (PLGA) nanoparticles prepared by high pressure homogenization for paclitaxel chemotherapy. *Int J Pharm*. 2007;342(1-2):208-14. doi: 10.1016/j.ijpharm.2007.04.031, PMID 17560058.
 27. FDA. Guidance for industry. Stab Test New Drug Subst Prod, U. S. Department of Health and Human Services, Food and Drug Administration. SubStance. 2003;Q1A(R2):1-22.
 28. Shriky B, Kelly A, Isreb M, Babenko M, Mahmoudi N, Rogers S. Pluronic F127 thermosensitive injectable smart hydrogels for controlled drug delivery system development. *J Colloid Interface Sci*. 2020;565:119-30. doi: 10.1016/j.jcis.2019.12.096, PMID 31945671.
 29. Nair AB, Shah J, Jacob S, Al-Dhubiab BE, Sreeharsha N, Morsy MA. Experimental design, formulation and *in vivo* evaluation of a novel topical in situ gel system to treat ocular infections. *PLOS ONE*. 2021;16(3):e0248857. doi: 10.1371/journal.pone.0248857, PMID 33739996.
 30. Vineetha K, Koland M. Investigation of a biodegradable injectable in situ gelling implantable system of rivastigmine tartrate. *Asian J Pharm*. 2017;2017:11-2.
 31. Baldassari S, Solari A, Zuccari G, Drava G, Pastorino S, Fucile C. Development of an injectable slow-release metformin formulation and evaluation of its potential antitumor effects. *Sci Rep*. 2018;8(1):3929. doi: 10.1038/s41598-018-22054-w, PMID 29500390.
 32. Dawood BY, Kassab HJ. Preparation and *in vitro* evaluation of naproxen as a pH sensitive ocular in situ gel. *Int J Appl Pharm*. 2019;11:37-44.
 33. Maheshwari M, Miglani G, Mali A, Paradkar A, Yamamura S, Kadam S. Development of tetracycline-serratiopeptidase-containing periodontal gel: formulation and preliminary clinical study. *AAPS PharmSciTech*. 2006;7(3):1-1076. doi: 10.1208/pt070376, PMID 17025256.
 34. Ng SF, Rouse J, Sanderson D, Eccleston G. A comparative study of transmembrane diffusion and permeation of ibuprofen across synthetic membranes using franz diffusion cells. *Pharmaceutics*. 2010;2(2):209-23. doi: 10.3390/pharmaceutics2020209, PMID 27721352.
 35. Sahoo S, Khodakiya A, Mithapara C, Ranjan SVS. Formulation and evaluation of sustained release in situ gel of loteprednol etabonate by using 32 full factorial design. *Aegaeum J*. 2020;8:566-84.
 36. Shen T, Yang Z. *In vivo* and *in vitro* evaluation of in situ gel formulation of pemirolast potassium in allergic conjunctivitis. *Drug Des Devel Ther*. 2021;15:2099-2107. doi: 10.2147/DDDT.S308448, PMID 34040348.

37. Kumar A, Sawant KK. Application of multiple regression analysis in optimization of anastrozole-loaded PLGA nanoparticles. *J Microencapsul.* 2014;31(2):105-14. doi: 10.3109/02652048.2013.808280, PMID 23883302.
38. Kumar A, Singh A, Flora SJS, Shukla R. Box-behnken design optimized TPGS coated bovine serum albumin nanoparticles loaded with anastrozole. *Curr Drug Deliv.* 2021;18(8):1148-59, 1136-47. doi: 10.2174/1567201818666210202104810, PMID 33530907.
39. Cesur S, Cam ME, Sayin FS, Gunduz O. Electrically controlled drug release of donepezil and BiFeO₃ magnetic nanoparticle-loaded PVA microbubbles/nanoparticles for the treatment of Alzheimer's disease. *J Drug Deliv Sci Technol.* 2022;67:102977. doi: 10.1016/j.jddst.2021.102977.
40. Shariatinia Z, Pourzadi N. Designing novel anticancer drug release vehicles based on mesoporous functionalized MCM-41 nanoparticles. *J Mol Struct.* 2021;1242:130754. doi: 10.1016/j.molstruc.2021.130754.
41. Aggarwal S, Ikram S. Zinc oxide nanoparticles-impregnated chitosan surfaces for covalent immobilization of trypsin: stability and kinetic studies. *Int J Biol Macromol.* 2022;207:205-21. doi: 10.1016/j.ijbiomac.2022.03.014, PMID 35259431.
42. Zidan AS, Sammour OA, Hammad MA, Megrab NA, Hussain MD, Khan MA. Formulation of anastrozole microparticles as biodegradable anticancer drug carriers. *AAPS PharmSciTech.* 2006;7(3):61. doi: 10.1208/pt070361, PMID 17025242.
43. Liu J, Jiang Z, Zhang S, Saltzman WM. Poly(ω -pentadecalactone-co-butylene-co-succinate) nanoparticles as biodegradable carriers for camptothecin delivery. *Biomaterials.* 2009;30(29):5707-19. doi: 10.1016/j.biomaterials.2009.06.061, PMID 19632718.
44. Inose T, Oikawa T, Tokunaga M, Yamauchi N, Nakashima K, Kato C. Development of composite nanoparticles composed of silica-coated nanorods and single nanometer-sized gold particles toward a novel X-ray contrast agent. *Materials Science and Engineering: B.* 2020;262:114716. doi: 10.1016/j.mseb.2020.114716.
45. Jia L, Guo L, Zhu J, Ma Y. Stability and cytocompatibility of silk fibroin-capped gold nanoparticles. *Mater Sci Eng C Mater Biol Appl.* 2014;43:231-6. doi: 10.1016/j.msec.2014.07.024, PMID 25175209.
46. Al Khateb K, Ozhmukhametova EK, Mussin MN, Seilkhanov SK, Rakhypbekov TK, Lau WM. In situ gelling systems based on pluronic F127/Pluronic F68 formulations for ocular drug delivery. *Int J Pharm.* 2016;502(1-2):70-9. doi: 10.1016/j.ijpharm.2016.02.027, PMID 26899977.
47. Alemdar M, Tuncaboylu DC, Batu HK, Temel BA. Pluronic based injectable smart gels with coumarin functional amphiphilic copolymers. *Eur Polym J.* 2022;177:111378. doi: 10.1016/j.eurpolymj.2022.111378.
48. Ahmad H, Ali Chohan T, Mudassir J, Mehta P, Yousef B, Zaman A. Evaluation of sustained-release in-situ injectable gels, containing naproxen sodium, using *in vitro*, *in silico* and *in vivo* analysis. *Int J Pharm.* 2022;616:121512. doi: 10.1016/j.ijpharm.2022.121512, PMID 35085730.
49. AS, Ahmed MG, Gowda BH J AS, Ahmed MG, Gowda BH J. Preparation and evaluation of in-situ gels containing hydrocortisone for the treatment of aphthous ulcer. *J Oral Biol Craniofacial Res.* 2021;11(2):269-76. doi: 10.1016/j.jobcr.2021.02.001.